
COVARIATE-DEPENDENT FUNCTIONAL PRINCIPAL COMPONENT ANALYSIS FOR SHM

A PREPRINT

Philipp Wittenberg 

Chair of Statistics and Data Science
Dept. of Mathematics and Statistics
School of Business, Economics and Social Sciences
Helmut Schmidt University
Hamburg, Germany
pwitten@hsu-hh.de

Lizzie Neumann 

Chair of Statistics and Data Science
Dept. of Mathematics and Statistics
School of Business, Economics and Social Sciences
Helmut Schmidt University
Hamburg, Germany
neumannl@hsu-hh.de

Kristof Maes 

Structural Mechanics Section
Dept. of Civil Engineering
Faculty of Engineering Science
KU Leuven
Leuven, Belgium
kristof.maes@kuleuven.be

Jan Gertheiss 

Chair of Statistics and Data Science
Dept. of Mathematics and Statistics
School of Business, Economics and Social Sciences
Helmut Schmidt University
Hamburg, Germany
gertheij@hsu-hh.de

March 20, 2026

Abstract

In Structural Health Monitoring (SHM), sensor measurements and derived features such as eigenfrequencies often exhibit systematic daily patterns and can therefore be naturally represented as functional data. Furthermore, these patterns are typically influenced by environmental factors, particularly temperature, which can substantially affect the observed system response. While most existing methods for removing environmental effects assume that confounding influences affect only the mean response, it has been shown that environmental and operational factors may also alter the covariance structure of the residual process. To address this limitation in a functional data monitoring framework, we incorporate so-called covariate-dependent functional principal component analysis (CD-FPCA), which allows eigenfunctions and eigenvalues of the residual process to vary smoothly with covariates such as temperature. The proposed methodology is illustrated using an extended version of the KW51 railway bridge eigenfrequency dataset. This case study suggests that accounting for covariate effects beyond the functional mean can improve the robustness of

the monitoring procedure, in particular by reducing environmentally induced (false) alarms under challenging low-temperature conditions.

Keywords: Environmental Variability, Functional Data Analysis, Natural Frequencies, Structural Health Monitoring, Statistical Learning

1 Introduction and Data

In structural health monitoring (SHM), it is well known that the system outputs, i.e., sensor measurements and derived damage-sensitive features (such as natural frequencies), change not only due to structural damage but also in response to environmental and operational variations (EOV), particularly due to temperature (Han et al., 2021; Wang et al., 2022). Additionally, system outputs often exhibit systematic, recurring daily patterns, making them well-suited to a functional data representation (Wittenberg et al., 2026). To account for environmental variability from a functional perspective, Wittenberg et al. (2025b) recently proposed the covariate-adjusted functional data analysis framework for SHM (CAFDA-SHM), which combines non-linear function-on-function regression with functional principal component analysis (FPCA) applied to the residual process. However, as with most existing methods for removing environmental effects, the CAFDA framework assumes that EOVs affect only the mean value of the system output. Recent works by Neumann et al. (2025b,a,c), however, demonstrated that EOVs may also affect higher-order moments, particularly the output’s (co-)variance structure. That is why incorporating conditional (co-)variance information into the monitoring framework could reduce the risk of false alarms and increase the probability of detecting actual damage.

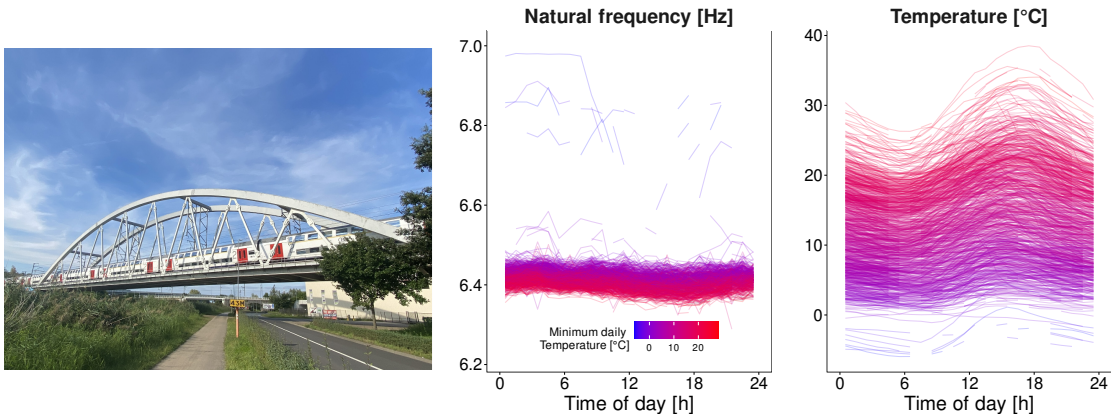


Figure 1. South view on bridge KW51 (left), considered profiles of natural frequencies (Mode 13, middle) and bridge surface temperature (right).

To illustrate both the functional perspective and the complex nature of environmental effects, we will consider the natural frequency dataset obtained from the long-term monitoring of railway bridge KW51 in Leuven, Belgium (Maes and Lombaert, 2020, 2021), see Figure 1 (left). The evolution of natural frequencies from 1st October 2018 to 30th September 2022 shows a significant temperature influence across most modes, particularly during frost periods. Apart from those, there was also a large influence of the retrofitting works (Maes et al., 2022). In this paper, we focus on the structure’s response during the period following

the retrofit, i.e., from 27th May 2019 to 30th September 2022. Note that this is a substantial extension of the original KW51 dataset presented in [Maes and Lombaert \(2020, 2021\)](#).

Figure 1 (middle) displays the data in functional data format, i.e., the natural frequency (Mode 13) is considered as a function of the time of day (0h to 24h). The tracked natural frequencies, however, contain substantial missing data due to the fact that not all modes were sufficiently excited to enable a 100% successful identification ([Maes and Lombaert, 2021](#)). We selected Mode 13 (the fifth-order vertical bending mode) because it shows a clear increase in natural frequency at cold temperatures, which is attributed to frost in the ballast layer. The fact that the data stream is characterized by gaps, together with highly nonlinear behavior in response to changing temperatures, poses another challenge for the modeling procedure. To address all these issues, this article extends the CAFDA framework by integrating a covariate-dependent version of functional principal component analysis (CD-FPCA) developed by [Jiang and Wang \(2010\)](#). CD-FPCA allows both the mean and covariance structure to depend on environmental covariates, thereby potentially improving robustness to environmental effects in SHM applications. The remainder of the article is structured as follows. Section 2 presents CD-FPCA and its integration with CAFDA-SHM. Section 3 reports the results on the KW51 data. Section 4 concludes the study and outlines potential extensions.

2 Methodology

2.1 Covariate-dependent FPCA

To address the challenges outlined in Section 1, we adapt the CD-FPCA approach developed by [Jiang and Wang \(2010\)](#). This approach consists of two components: a systematic part considering the mean function and a stochastic part comprising random components that reflect the covariance structure. The former, as discussed in [Wittenberg et al. \(2025b,a\)](#), can be modeled using functional regression that incorporates the effects of covariates on the mean. The latter, unlike classical FPCA, explicitly includes a covariance structure that depends on covariates. The original CD-FPCA works as follows. The covariate z may be a one-dimensional, scalar quantity like the minimum daily temperature as used for coloring in Figure 1 (middle/right), or multivariate, vector-valued; however, due to the so-called ‘‘curse of dimensionality’’, only a low-dimensional covariate is practically feasible. To keep things simple, we will focus on a one-dimensional z . Then, it is assumed that the quantity of interest $y(t, z)$, here, the natural frequency y at time $t \in \mathcal{T}$ for a given z , has the form

$$y(t, z) = \mu(t, z) + \sum_{r=1}^{\infty} \xi_r \phi_r(t, z), \quad (1)$$

where $\mu(t, z)$ is the (conditional) mean of y at time t for a given z ; $\phi_r(t, z)$, $r = 1, 2, \dots$, are the eigenfunctions of the (conditional) covariance operator $\Gamma(s, t, z) = \text{Cov}(y(s, z), y(t, z))$, and ξ_r are uncorrelated random scores with mean 0 and variance $\nu_r(z)$, with $\nu_1(z) \geq \nu_2(z) \geq \dots \geq 0$ being the eigenvalues of $\Gamma(s, t, z)$. The (observable) system output $u_{ij} = y(t_{ij}, z_i) + \epsilon_{ij}$ represents the j th observation on day i of the (underlying) y , recorded at a time point $t_{ij} \in \mathcal{T}$, $\mathcal{T} = (0h, 24h]$, $i = 1, \dots, n$, and $j = 1, \dots, n_i$. Each observation has an associated covariate $z_i \in \mathbb{R}$ (here, minimum daily temperature) and additionally, an independent and identically distributed measurement error/white noise ϵ_{ij} with mean zero and constant variance σ^2 . Typically, the sum in (1) is truncated at some value m resulting in the model

$$u_{ij} = \mu(t_{ij}, z_i) + \sum_{r=1}^m \xi_{ir} \phi_r(t_{ij}, z_i) + \epsilon_{ij}, \quad (2)$$

with scores ξ_{ir} and measurement errors ϵ_{ij} being mutually independent.

In a real-world SHM scenario, however, the temperature is not only observed in terms of its daily minimum (or other aggregated values), but as a profile over the entire day (compare Figure 1, right), and the (expected) natural frequency at time t should rather depend on the material temperature $x(t)$ at the very time t than the daily minimum temperature z . Following Wittenberg et al. (2025b), we hence replace $\mu(t, z)$ in (1) by $\mu(t, x(t)) = \alpha_0 + \tilde{\alpha}(t) + f(x(t))$ and $\mu(t_{ij}, z_i)$ in (2) by $\mu(t_{ij}, x_i(t_{ij})) = \alpha_0 + \tilde{\alpha}(t_{ij}) + f(x_i(t_{ij}))$, respectively, where f describes the, concurrent and potentially nonlinear, effect of the (material) temperature. The overall constant α_0 together with the so-called (centered) functional intercept $\tilde{\alpha}$ model (potential) recurring daily patterns that are, e.g., induced by other (unobserved) covariates and cannot be explained through the temperature alone. Concerning the covariance operator $\Gamma(s, t, z)$, it is still assumed that the aggregated z is sufficient to account for the higher-order effects beyond the mean μ . A key step in the corresponding CD-FPCA procedure is then the estimation of the covariate-dependent covariance function $\Gamma(s, t, z)$, from which covariate-specific eigenvalues and eigenfunctions follow via the associated eigendecomposition. The covariance estimator is obtained by smoothing the raw covariances

$$c_{ijk} = (u_{ij} - \hat{\mu}(t_{ij}, x_i(t_{ij}))) (u_{ik} - \hat{\mu}(t_{ik}, x_i(t_{ik}))), \quad (3)$$

where the mean function μ is estimated in the framework of functional additive mixed models (Ivanescu et al., 2015; Scheipl et al., 2016; Greven and Scheipl, 2017) as described in Wittenberg et al. (2025b). For a one-dimensional z , estimating $\Gamma(t, s, z)$ requires smoothing a three-dimensional surface of c_{ijk} over (t_{ij}, t_{ik}, z_i) for all $j, k = 1, \dots, n_i$, $i = 1, \dots, n$. As in Jiang and Wang (2010), we employ a local-linear smoother in terms of

$$\begin{aligned} \hat{\Gamma}(t, s, z) &= \hat{\beta}_0, \quad \text{where} \\ \hat{\beta} &= \arg \min_{\beta = (\beta_0, \beta_1, \beta_2, \beta_3)^\top} \left\{ \sum_{i=1}^n \sum_{1 \leq j \neq k \leq n_i} K_3 \left(\frac{t - t_{ij}}{h_t}, \frac{s - t_{ik}}{h_t}, \frac{z - z_i}{h_z} \right) \right. \\ &\quad \left. \times [c_{ijk} - (\beta_0 + \beta_1(t_{ij} - t) + \beta_2(t_{ik} - s) + \beta_3(z_i - z))]^2 \right\}, \end{aligned} \quad (4)$$

with K_3 being a three-dimensional kernel function. The bandwidths h_t, h_z can be selected via k -fold cross-validation; see, e.g., Petersen et al. (2019).

2.2 Estimation and monitoring of the scores

Assuming normally distributed principal component scores and measurement errors, the scores can be estimated following the approach of Yao et al. (2005)

$$\hat{\xi}_{ir} = \hat{\nu}_r(z_i) \hat{\phi}_{ir}^\top \hat{\Sigma}_i^{-1} (\mathbf{u}_i - \hat{\boldsymbol{\mu}}_i) \quad r = 1, \dots, m, \quad (5)$$

where $\mathbf{u}_i = (u_{i1}, \dots, u_{i, n_i})^\top$, $\hat{\boldsymbol{\mu}}_i = (\hat{\mu}(t_{i1}, x_i(t_{i1})), \dots, \hat{\mu}(t_{i, n_i}, x_i(t_{i, n_i})))^\top$, $\hat{\phi}_{ir} = (\hat{\phi}_r(t_{i1}, z_i), \dots, \hat{\phi}_r(t_{i, n_i}, z_i))^\top$, $(\hat{\Sigma}_i)_{j,k} = \hat{\Gamma}(t_{ij}, t_{ik}, z_i) + \hat{\sigma}^2 \delta_{jk}$, and $\delta_{jk} = 1$ if $j = k$ and 0 otherwise. The covariate-dependent eigensystem $\{\hat{\phi}_r(\cdot, z), \hat{\nu}_r(z)\}$, mean function μ , and error variance σ^2 are estimated from Phase I/training data and, in theory, both $\hat{\phi}_r(\cdot, z)$ and $\hat{\nu}_r(z)$ are smooth functions of z . In practice, to save computational time during monitoring, they are already evaluated over the relevant range of the covariate on a reasonably fine grid $z^{(1)}, \dots, z^{(G)}$ during training. In the actual monitoring phase, so-called Phase II, for a new day $l = 1, 2, \dots$ with covariate z_l , we select the nearest grid point $z^{(g^{(l)})}$ and use the corresponding eigenfunctions and eigenvalues. As discussed in Section 2.1, under IC conditions the CD-FPCA scores ξ_{lr} obtained through (5) satisfy $\mathbb{E}(\xi_{lr} \mid z_l) = 0$ and $\text{Var}(\xi_{lr} \mid z_l) = \nu_r(z_l)$ with approximately uncorrelated

components. Consequently, raw scores are not directly comparable across covariate levels, because their dispersion changes systematically with the environmental state. In our application, however, the model-based eigenvalue curves $\hat{\nu}_r(z)$ were not sufficiently stable across the covariate range and did not consistently match the empirical dispersion of the estimated scores in (5). We therefore introduced a post-FPCA calibration step based on the Phase I scores. For each retained component r , we estimated a smooth mean curve $\hat{m}_r(z)$ using a generalized additive model (GAM; Wood, 2017) and subtracted it from the scores as a covariate-dependent mean correction. The squared centered scores were then fitted by a GAM with log link, yielding a positive variance estimate $\hat{v}_r(z)$. The standardized monitoring inputs were thus defined as

$$X_{lr} = \frac{\hat{\xi}_{lr} - \hat{m}_r(z_l)}{\sqrt{\hat{v}_r(z_l)}}, \quad r = 1, \dots, m, \quad (6)$$

and collected in $\mathbf{X}_l = (X_{l1}, \dots, X_{lm})^\top$ for the subsequent application in a multivariate control chart.

2.3 MEWMA control chart on standardized scores

To detect small-to-moderate persistent changes, the Multivariate Exponentially Weighted Moving Average (MEWMA) chart of Lowry et al. (1992) to the standardized score vectors $\{\mathbf{X}_l\}$ is applied. The MEWMA state is defined recursively as

$$\mathbf{Z}_l = \lambda \mathbf{X}_l + (1 - \lambda) \mathbf{Z}_{l-1}, \quad \mathbf{Z}_0 = \mathbf{0}, \quad 0 < \lambda \leq 1, \quad (7)$$

where smaller values of λ yield stronger smoothing and hence greater sensitivity to sustained deviations. Under ideal in-control conditions with $\text{Cov}(\mathbf{X}_l) = \mathbf{I}_m$, the stationary covariance of \mathbf{Z}_l is $\mathbf{\Lambda}_Z = \frac{\lambda}{2-\lambda} \mathbf{I}_m$, which leads to the monitoring statistic

$$T_l^2 = \mathbf{Z}_l^\top \mathbf{\Lambda}_Z^{-1} \mathbf{Z}_l = \frac{2-\lambda}{\lambda} \mathbf{Z}_l^\top \mathbf{Z}_l. \quad (8)$$

An alarm is raised whenever $T_l^2 > h_4$, where h_4 is selected to attain a prescribed in-control ‘‘average run length’’ ARL_0 . Because the standardized Phase I scores could still exhibit mild residual serial dependence, we calibrated h_4 using a moving-block bootstrap, as in Neumann et al. (2025c), rather than relying exclusively on the i.i.d. Gaussian approximation. Bootstrap sequences are generated by repeatedly sampling contiguous blocks of consecutive daily score vectors \mathbf{X}_i of length b from Phase I data. For the control limit h_4 , the run length was defined as $\text{RL}(h_4) = \inf\{i \geq 1 : T_i^2 > h_4\}$, and the in-control ARL was estimated by averaging this run length over 100,000 bootstrap replicates. The final control limit was then obtained numerically by utilizing a grid search to match the desired target ARL.

3 Modeling and Monitoring Results on the KW51 Extended Data

The complete post-retrofitting period comprised 1101 days. The observed Mode 13 frequency profiles were strongly incomplete, only 17 days contained complete 24-point trajectories, while 1084 days exhibited at least one missing profile observation. On average, 16.5 frequency observations per day were available, ranging from 0 to 24, which corresponds to an overall missingness rate of 31.2%. Temperature measurements were also incomplete, but less sparse overall, with an average of 19.0 observations per day. Between 18th May 2021 and 27th May 2021, maintenance works were carried out on the KW51 railway bridge. During this period, the northern rails of tracks A and B were replaced. The minimum daily temperature spanned a fairly narrow mild-temperature band between 8.7°C and 11.2°C. The new rails were delivered on 18th May 2021 and temporarily stored on the sleepers next to the existing rails to be renewed. This temporary storage

corresponded to an additional distributed mass of approximately $2 \times 60 \text{ kg/m}$ along the bridge and may therefore have affected its dynamic behavior. In the night from 23rd May 2021 to 24th May 2021, the outer rail of track A was renewed. In the night from 26th May 2021 to 27th May 2021, the outer rail of track B was renewed, and the old rails for both tracks were removed. In the present study, Phase I extended from 27th May 2019, immediately after completion of the retrofitting, to 31st March 2021, whereas Phase II covered the period from 1st April 2021 to 30th September 2022. The maintenance period lies within Phase II and serves as the event window for evaluating the monitoring results obtained with both the ‘old’ CAFDA-SHM framework and the new CD-FPCA-based approach.

3.1 Temperature effects on the mean and (co-)variance

Figure 2 (left) shows the estimated (fixed) covariate effect $f(x(t))$ on the mean μ . The functional intercept (not shown) is nearly flat, indicating that after accounting for temperature, (almost) no additional systematic time-of-day structure remains in the mean response. However, the estimated temperature effect is very strong and clearly nonlinear, particularly in the lower temperature range. This suggests that temperature is the dominant driver of the expected frequency profile, with more severe changes occurring under cold conditions. These lower-temperature regimes are of particular importance for the subsequent monitoring analysis, since they are sparsely represented in the data and are associated with increased instability and environmentally induced alarms. Overall, the fixed-effects model explains approximately $R^2 \approx 0.80$ of the observed variation.

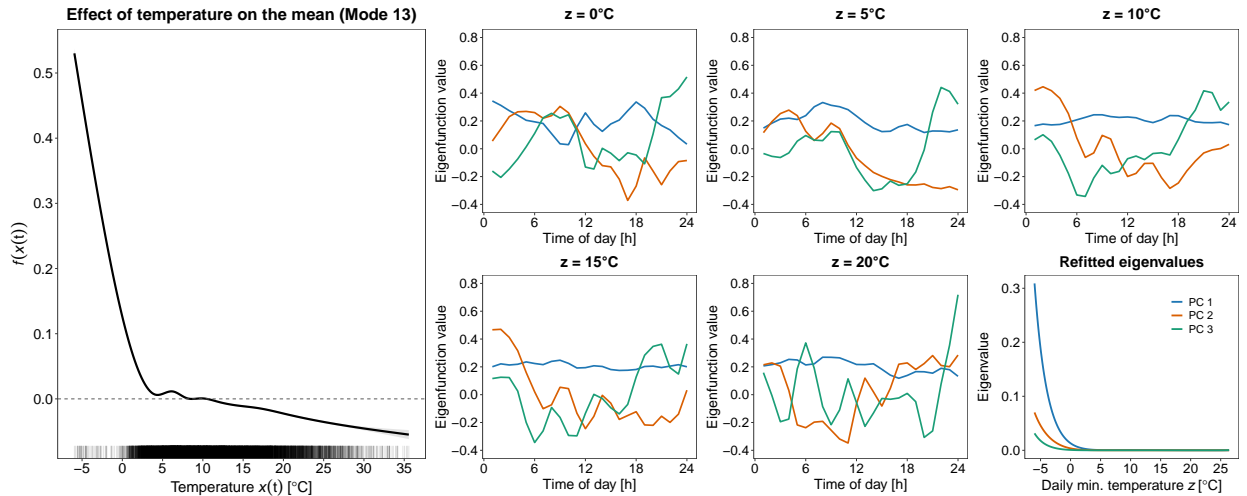


Figure 2. Temperature effect on the mean μ (left), covariate-dependent eigenfunctions (middle) and eigenvalues (right) for various temperatures.

The remaining plots in Figure 2 show, as an example, the first three eigenfunctions for five distinct temperatures between 0°C and 20°C , along with the corresponding eigenvalues as smooth functions of the daily minimum temperature. The eigenvalues, which correspond to the variances of the respective (functional) principal component scores, decrease monotonically with increasing temperature. The eigenfunctions also vary with temperature but appear rather wiggly, making them more difficult to interpret. At least, the first component (blue) consistently captures the overall level of the residual process because it is basically constant across both temperature and time.

3.2 Monitoring results

For both control charts (using either CAFDA or CD-FPCA), we set $\lambda = 0.4$ and targeted an in-control average run length of $ARL_0 = 500$, which is well aligned with the scale of the available reference period and implies approximately one expected false alarm over an in-control run of similar length. In addition, both charts used the same fixed-effects model as described in Subsection 3.1.

For the CAFDA-SHM, the control limit was determined under the i.i.d. assumption as in [Wittenberg et al. \(2025b\)](#). The estimated number of functional principal components was $m = 3$, corresponding to a fraction of explained variance of 95%, and the resulting alarm threshold was $h_4 = 14.6$. Using the full temperature spectrum without additional robustification in Phase I, the CAFDA-SHM chart exhibited a pronounced cold-temperature issue in February 2021 as displayed in Figure 3 (top). In total, 17 alarms were observed in Phase I, of which 14 occurred on days with temperatures at or below 2°C . In Phase II, the pattern was more mixed but still showed a substantial temperature-related component. A total of 5 alarms were recorded, with 3 occurring near freezing temperatures. The remaining 2 alarms occurred in October under comparatively mild conditions of around 12°C . At the same time, the chart did not detect the bridge intervention event highlighted in grey in Figure 3. For the CD-FPCA approach, the control limit was set

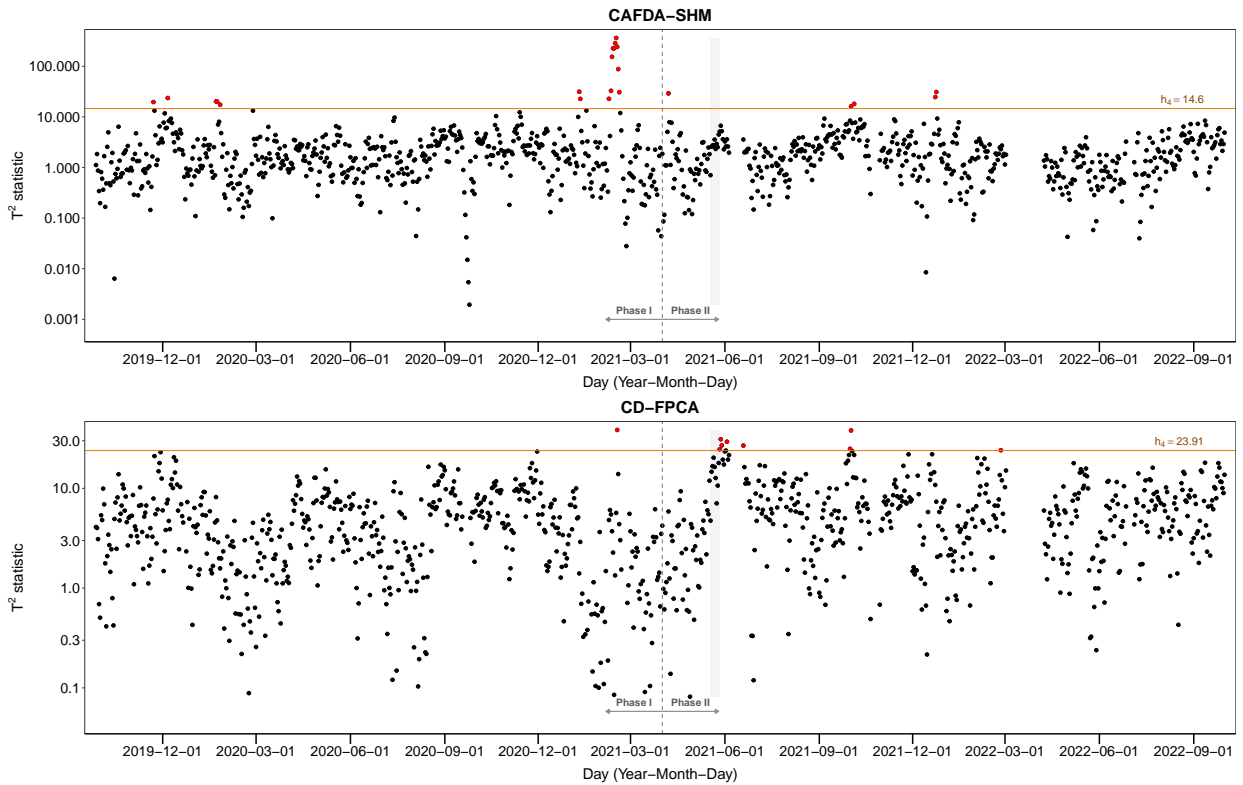


Figure 3. MEWMA control charts for the CAFDA-SHM (top) and the proposed CD-FPCA framework (bottom).

to $h_4 = 23.91$. Its calibration required a moving-block bootstrap with block length $b = 3$, due to the weak but non-negligible serial dependence observed in the empirical autocorrelation function of the standardized scores in (6). The resulting MEWMA chart is shown in Figure 3 (bottom). In Phase I, the chart signaled only a single false alarm on 16th February 2021 (at around 2.3°C). In Phase II, eight signals were detected. The first alarm occurred on 27th May 2021, i.e., on the last day of the bridge intervention event, and was

followed by two further signals on the next two consecutive days. The remaining signals, on 3rd June, 19th June, 1st and 2nd October in 2021, and on 25th February 2022 under comparatively milder temperatures, are likely false alarms. Compared with CAFDA-SHM, this indicates a substantial reduction of environmentally induced (false) alarms in Phase I while still yielding a detection during the event window.

4 Discussion and Outlook

The case study from Section 3 represented a challenging real-world setting. The tracked natural-frequency profiles are sparsely and irregularly observed, exhibit substantial missingness, and the anomaly associated with the bridge intervention is comparatively small. In addition, low-temperature regimes, which are particularly relevant for the covariance structure, are less densely represented. These features make the dataset informative for assessing the robustness of the proposed approach, but they also limit the extent to which a sharp separation between in-control and out-of-control behavior can be expected. Analyses in the pre-retrofitting setting, not included in this paper, indicate a stronger performance in the presence of a substantially larger shift during the retrofitting period. Thus, the monitoring performance observed here should be interpreted in light of the particular difficulties of the (new) post-retrofitting case study.

Further, the proposed CD-FPCA framework has certain limitations and suggests avenues for future research. First, the new method was implemented only for a scalar covariate, the minimum daily temperature. An important extension would therefore be a fully functional covariate-dependent FPCA that accounts for the complete temperature profile rather than a scalar summary. Second, the present analysis employs a comparatively simple functional mean model and does not incorporate further environmental or operational variables. The proposed approach was also applied only to a single system output (Mode 13), although [Wittenberg et al. \(2025a\)](#) showed that related monitoring concepts can be extended to multivariate functional data streams. Finally, instead of the local-linear three-dimensional smoother used here, alternative estimators such as the spline-based covariate-dependent FPCA approach of [Ding et al. \(2022\)](#) could be explored in future work.

Software

The statistical analyses were conducted in the open-source software R ([R Core Team, 2025](#)). Functional additive (mixed) models were fitted with the `mgcv` package ([Wood, 2017](#)). In addition, the CD-FPCA algorithm, originally implemented in MATLAB ([The MathWorks, Inc., 2022](#)), was ported to Julia ([Bezanson et al., 2017](#)) and used for the corresponding analyses.

Acknowledgements

This research paper out of the project ‘SHM – Digitalisierung und Überwachung von Infrastrukturbauwerken’ is funded by dtec.bw – Digitalization and Technology Research Center of the Bundeswehr, which we gratefully acknowledge. dtec.bw is funded by the European Union – NextGenerationEU.

References

J. Bezanson, A. Edelman, S. Karpinski, and V. B. Shah. Julia: A fresh approach to numerical computing. *SIAM Review*, 59(1):65–98, 2017. doi:[10.1137/141000671](https://doi.org/10.1137/141000671).

- F. Ding, S. He, D. E. Jones, and J. Z. Huang. Functional PCA with covariate-dependent mean and covariance structure. *Technometrics*, 64(3):335–345, 2022. doi:[10.1080/00401706.2021.2008502](https://doi.org/10.1080/00401706.2021.2008502).
- S. Greven and F. Scheipl. A general framework for functional regression modelling. *Statistical Modelling*, 17(1-2):1–35, 2017. doi:[10.1177/1471082X16681317](https://doi.org/10.1177/1471082X16681317).
- Q. Han, Q. Ma, J. Xu, and M. Liu. Structural health monitoring research under varying temperature condition: a review. *Journal of Civil Structural Health Monitoring*, 11:149–173, 2021. doi:[10.1007/s13349-020-00444-x](https://doi.org/10.1007/s13349-020-00444-x).
- A. Ivanescu, A. Staicu, and F. Scheipl. Penalized function-on-function regression. *Computational Statistics*, 30(2):539–568, 2015. doi:[10.1007/s00180-014-0548-4](https://doi.org/10.1007/s00180-014-0548-4).
- C.-R. Jiang and J.-L. Wang. Covariate adjusted functional principal components analysis for longitudinal data. *The Annals of Statistics*, 38(2):1194–1226, 2010. doi:[10.1214/09-AOS742](https://doi.org/10.1214/09-AOS742).
- C. A. Lowry, W. H. Woodall, C. W. Champ, and S. E. Rigdon. A Multivariate Exponentially Weighted Moving Average Control Chart. *Technometrics*, 34(1):46–53, 1992. doi:[10.2307/1269551](https://doi.org/10.2307/1269551).
- K. Maes and G. Lombaert. Monitoring data for railway bridge KW51 in Leuven, Belgium, before, during, and after retrofitting. V1.0, 2020.
- K. Maes and G. Lombaert. Monitoring Railway Bridge KW51 Before, During, and After Retrofitting. *Journal of Bridge Engineering*, 26(3):04721001, 2021. doi:[10.1061/\(ASCE\)BE.1943-5592.0001668](https://doi.org/10.1061/(ASCE)BE.1943-5592.0001668).
- K. Maes, L. Van Meerbeeck, E. P. Reynders, and G. Lombaert. Validation of vibration-based structural health monitoring on retrofitted railway bridge KW51. *Mechanical Systems and Signal Processing*, 165:108380, 2022. doi:[10.1016/j.ymssp.2021.108380](https://doi.org/10.1016/j.ymssp.2021.108380).
- L. Neumann, P. Wittenberg, and J. Gertheiss. Confidence Intervals for Conditional Covariances of Natural Frequencies. In M. Döhler, A. Mélot, and M. A. López, editors, *Proceedings of the 11th International Operational Modal Analysis Conference (IOMAC 2025)*, pages 742–749, Rennes, France, 2025a. ISBN 978-84-09-75120-4.
- L. Neumann, P. Wittenberg, A. Mendler, and J. Gertheiss. Confounder-adjusted covariances of system outputs and applications to structural health monitoring. *Mechanical Systems and Signal Processing*, 224:111983, 2025b. doi:[10.1016/j.ymssp.2024.111983](https://doi.org/10.1016/j.ymssp.2024.111983).
- L. Neumann, P. Wittenberg, A. Mendler, and J. Gertheiss. Signal and feature reconstruction in structural health monitoring under varying environmental conditions. *Preprint*, 2025c. doi:[10.2139/ssrn.5748533](https://doi.org/10.2139/ssrn.5748533). Submitted to *Engineering Structures*.
- A. Petersen, S. Deoni, and H.-G. Müller. Fréchet estimation of time-varying covariance matrices from sparse data, with application to the regional co-evolution of myelination in the developing brain. *The Annals of Applied Statistics*, 13(1):393–419, 2019. doi:[10.1214/18-AOAS1195](https://doi.org/10.1214/18-AOAS1195).
- R Core Team. *R: A Language and Environment for Statistical Computing*. R Foundation for Statistical Computing, Vienna, Austria, 2025. URL <https://www.R-project.org/>.
- F. Scheipl, J. Gertheiss, and S. Greven. Generalized functional additive mixed models. *Electronic Journal of Statistics*, 10(1):1455–1492, 2016. doi:[10.1214/16-EJS1145](https://doi.org/10.1214/16-EJS1145).
- The MathWorks, Inc. MATLAB version: 9.13.0 (R2022b), 2022. URL <https://www.mathworks.com>.

- Z. Wang, D.-H. Yang, T.-H. Yi, G.-H. Zhang, and J.-G. Han. Eliminating environmental and operational effects on structural modal frequency: A comprehensive review. *Structural Control and Health Monitoring*, 29(11):e3073, 2022. doi:[10.1002/stc.3073](https://doi.org/10.1002/stc.3073).
- P. Wittenberg, A. Mendler, S. Knoth, and J. Gertheiss. Multivariate Long-Term Profile Monitoring with Application to the KW51 Railway Bridge. In Á. Cunha and E. Caetano, editors, *Experimental Vibration Analysis for Civil Engineering Structures*, pages 463–472, Cham, 2025a. Springer Nature Switzerland. doi:[10.1007/978-3-031-96114-4_48](https://doi.org/10.1007/978-3-031-96114-4_48).
- P. Wittenberg, L. Neumann, A. Mendler, and J. Gertheiss. Covariate-adjusted functional data analysis for structural health monitoring. *Data-Centric Engineering*, 6:e27, 2025b. doi:[10.1017/dce.2025.18](https://doi.org/10.1017/dce.2025.18).
- P. Wittenberg, S. Knoth, and J. Gertheiss. Structural Health Monitoring with Functional Data: Two Case Studies. In S. Knoth and W. Schmid, editors, *Frontiers in Statistical Quality Control 14*, Cham, 2026. Springer Nature Switzerland (forthcoming). Preprint available from arXiv. doi:[10.48550/arXiv.2406.01262](https://doi.org/10.48550/arXiv.2406.01262).
- S. N. Wood. *Generalized Additive Models: An Introduction with R*. CRC Press, Boca Raton, 2nd. edition, 2017.
- F. Yao, H.-G. Müller, and J.-L. Wang. Functional Data Analysis for Sparse Longitudinal Data. *Journal of the American Statistical Association*, 100(470):577–590, 2005. doi:[10.1198/016214504000001745](https://doi.org/10.1198/016214504000001745).